Appl. Phys. A 73, 27–33 (2001) / Digital Object Identifier (DOI) 10.1007/s003390100699

Applied Physics A
Materials
Science & Processing

Invited paper

Cavity ring-down spectroscopy of CH and CD radicals in a diamond thin film chemical vapor deposition reactor

U. Lommatzsch[1], E.H. Wahl[2], D. Aderhold[1], T.G. Owano[2], C.H. Kruger[2], R.N. Zare[1,*]

[1] Department of Chemistry, Stanford University, Stanford, CA 94305, USA
[2] Department of Mechanical Engineering, Stanford University, Stanford, CA 94305, USA

Received: 21 August 2000/Accepted: 23 August 2000/Published online: 23 May 2001 –

Abstract. A mixture of H_2 and CH_4 is passed over a hot-wire tungsten filament in a diamond thin film chemical vapor deposition reactor. The resulting CH radicals are measured in absorption using cavity ring-down spectroscopy (CRDS). The concentration of the CH radicals increases as the filament is approached. The rotational temperature measurements indicate a large temperature discontinuity between the filament and the CH in the gas phase. The pathways for CH production were investigated by replacing H_2 by D_2 in the feed gas mixture, which resulted in the exclusive production of CD. From this observation it is concluded that rapid H/D isotope exchange dominates in the gas phase. Nonperiodic temporal oscillations in the CH concentration are observed when a rhenium filament is used in place of a tungsten filament. The oscillations are attributed to the nonperiodic changes in the amount of carbon at the filament surface.

PACS: 81.15.Gh; 82.80.Ch; 82.40.Bj

Cavity ring-down spectroscopy (CRDS) is a novel laser-based method for absorption measurements of species that either weakly absorb or exist at low concentrations [1, 2]. In this study CRDS is used as a gas-phase diagnostic in a diamond thin film chemical vapor deposition (CVD) reactor. The high sensitivity (which can approach the shot-noise limit [3]), the simple quantification without the need for a calibration procedure, and the capability of spatial resolution make this technique especially well suited for this purpose. Since its invention, CRDS has been used to study a variety of molecules in CVD reactors [4–6]. Competitive diagnostic methods that have been used in diamond CVD reactors are laser-induced fluorescence (LIF) [7–9], optical emission spectroscopy (OES) [10], coherent anti-Stokes Raman spectroscopy (CARS) [11, 12], resonance-enhanced multiphoton ionization (REMPI) [13–17], third-harmonic generation [18, 19], degenerate four-wave mixing (DFWM) [20], mass spectrometry [21–24], vacuum UV- [25–27], IR-absorption [28], and gas chromatography (GC) [29, 30]. One of the main disadvantages of these other methods is the need for a calibration procedure to derive (absolute) concentrations.

In the simplest implementation of CRDS, a short light-pulse from a laser is injected into a high-finesse linear resonator built from two highly reflective mirrors. The absorbance of a sample is measured by observing the decay of light intensity within the optical resonator that encloses the sample [2]. Detecting the light exiting through one of the mirrors is a way of monitoring the intensity decay within the cavity. For a sufficiently short laser pulse, the light inside the cavity can be visualized as a light pulse bouncing back and forth between both mirrors. On each round-trip a constant fraction of the light inside the resonator is transmitted through the mirrors. With a fast photodetector a train of pulses whose successive intensities decay exponentially would be observed. A slow detector shows only the envelope of the decaying train of pulses. Thus the intensity $I(t)$ at time t is related to the initial intensity I_0 by

$$I(t) = I_0 \exp(-t/\tau) \tag{1}$$

where τ is the ring-down lifetime. The value of τ is inversely proportional to the losses of the empty resonator (e.g., mirror and scattering losses) and to losses from absorption of gaseous species present within the resonator. By measuring the ring-down lifetimes τ and τ_0 for a cavity with and without a sample present, respectively, the sample absorbance A is determined according to

$$A = \frac{t_r}{2}\left(\frac{1}{\tau} - \frac{1}{\tau_0}\right) \tag{2}$$

where $t_r = 2d/c$ is the round-trip transit time, c is the speed of light, and d is the distance between the two mirrors. In (2) the refractive index is assumed to be unity.

High-accuracy measurements become possible if the bandwidth and mode structure of the laser, the mode structure of the cavity, and the input mode coupling are carefully considered [31–33]. To avoid distortion of the exponential decay

*Corresponding author.
(Fax: +1-650/723-9262, E-mail: zare@stanford.edu)

the lowest-order transverse electromagnetic mode (TEM_{00}) of the optical resonator should be preferentially excited. Furthermore the laser bandwidth must be smaller than the absorption features of interest but larger than the free spectral range of the cavity. The first condition assures that the absorption losses for the spectral content of the laser pulse are all equal and the second condition avoids missing spectral features caused by the frequency-selective nature of the resonator.

If the conditions above are fulfilled, Beer's law (3) can be employed to extract the number density N from the sample absorbance A with high accuracy provided the absorption cross section σ and the path length l are known (for a homogeneous sample distribution between both mirrors the relation $l = d$ holds).

$$A = \sigma \cdot N \cdot l \tag{3}$$

The high sensitivity of CRDS is the result of its insensitivity to shot-to-shot fluctuations in laser intensity and the long absorption path length. The spatial resolution of this line-of-sight technique is limited by the diameter of the laser beam inside the optical cavity that is given by the mode profile of the excited transverse mode(s). Furthermore, measurements are restricted to regions some millimeters away from surfaces in order to avoid diffraction effects [34].

Diamond thin films are usually produced by CVD in a plasma, microwave, flame or hot-filament (HF-CVD) reactor [35, 36], but widespread applications of diamond thin films are limited by its high production cost. A rational attempt to improve film quality and growth rates requires the understanding of the reaction mechanisms and the identification of the precursor(s) in the diamond growth. In experimental studies HF-CVD reactors are commonly used because of their relative ease of operation and to facilitate comparison with theoretical simulations. In a HF-CVD reactor a mixture of hydrogen and methane flows over a hot wire, for the primary purpose of H-atom production. The hydrogen atoms predominantly drive the gas phase chemistry involving species such as C_xH_y with $x = 1-10$ [37], e.g., by the hydrogen shift reactions shown in (4):

$$CH_y + H \leftrightarrows CH_{y-1} + H_2 \quad \text{where } y = 1-4 \tag{4}$$

The diamond deposition occurs on a substrate in close proximity to the filament. The main precursor(s) in the diamond growth is (are) still not positively identified, but CH_3 and C_2H_2 are believed to be the most likely candidates [36, 38].

In this paper the spatial concentration distribution between filament and substrate of the short-lived radical CH is examined by CRDS. The gas temperature in the reactor is derived from a Boltzmann plot for the CH radical. To further elucidate the formation mechanism of the CH radical an isotope-exchange experiment was performed. As a result the direct absorption spectrum of the CD radical is reported here. Finally, the long-term stabilities of CH concentrations using filaments made out of tungsten and rhenium are compared.

1 Experimental

1.1 CVD reactor

The CVD system is housed in a vacuum chamber consisting of a 5-way stainless-steel cross 10.2 cm in diameter. A two-stage mechanical pump (E2M40, Edwards) evacuates the chamber. A capacitance manometer (MKS Instruments PDR-C-2 C, Burlington, MA.) measures the pressure. The reactor is maintained at a pressure of 2666 Pa (20 Torr) and is filled with a mixture of 1% methane in hydrogen (Praxair) at a flow rate of 100 sccm, which is adjusted by a flow controller (Hastings Power Supply, Model 200). The straight tungsten or rhenium filament (Thermo Shield, Los Altos, Calif.) is 20 mm long and 0.2 mm in diameter. It is mounted on two tungsten posts, that are fixed to water-cooled copper electrodes (Fig. 1). It is resistively heated with a dc current to a brightness temperature of 2400–2500 K, which is monitored by a disappearance pyrometer (Micro-optical pyrometer, Pyrometer Inc., Bergenfield, N.J.) through a quartz window. The pyrometer is calibrated with a tungsten target at known temperatures. The electrical power consumption at the filament

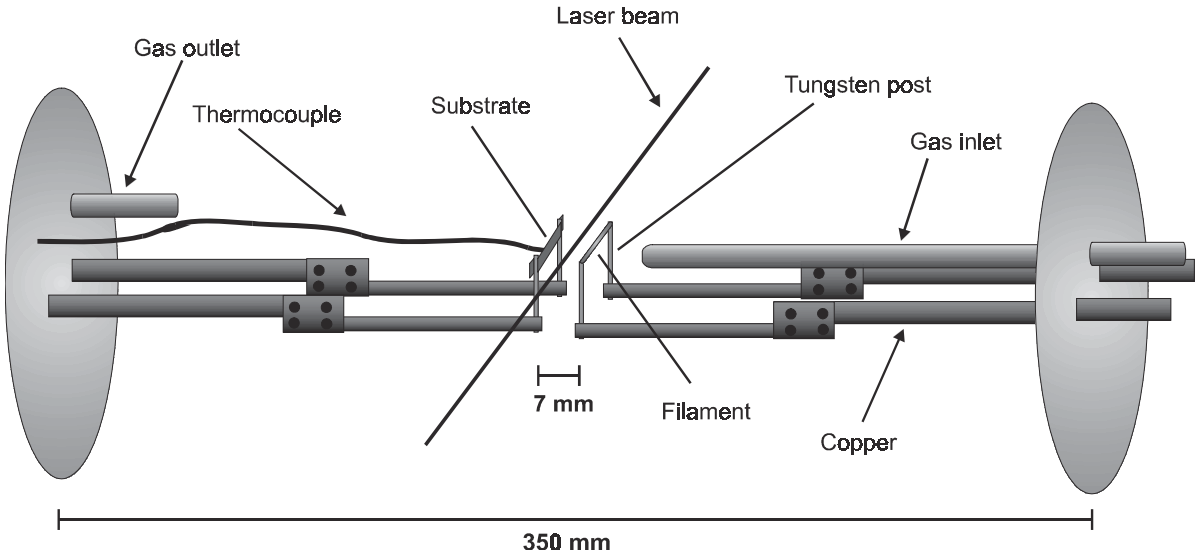

Fig. 1. The interior of the CVD reactor with the filament parallel to the interrogating laser beam and the substrate. The gas inlet is centered on the filament

is continuously monitored by voltage and current measurements. With a feedforward control the voltage at the filament is regulated to maintain constant power consumption. The filament, by a 90 degree rotation, can be positioned either parallel or perpendicular to the beam path in the optical cavity. The distance between the filament and the light path is adjusted by a translation stage that moves the reactor relative to the optical light-path. The distance is measured by a caliper whose zero position is taken to be the center of a plot of the ring-down time versus filament position. This procedure is performed for the cold and then hot filament to avoid uncertainties caused by thermal expansion. A 220-μm-thick molybdenum substrate strip with a surface dimension of 4×20 mm can be positioned at a distance of 7 mm from the filament and in the same orientation as the filament. To control the substrate temperature it is resistively heated, while its temperature is monitored by a K-type thermocouple welded to the rear surface.

1.2 Optical setup

The stable optical resonator consists of two mirrors (Los Gatos Research, Mountain View, Calif.) with a 6-m radius of curvature and a diameter of 2 cm. The spacing between the mirrors is 65.1 cm. The maximum reflectivity R of the mirrors occurs at 430 nm with $R = 99.993\%$. The value of R is directly determined from the ring-down lifetime for the empty cavity (~ 20 Torr of nitrogen). The mirrors can be finely adjusted by 3-axis mounts (Los Gatos Research, Mountain View, Calif.) which are mounted on 3.8-cm-thick aluminum blocks connected by four stainless-steel rods 2 cm in diameter. The reactor is mounted between the plates by means of flexible bellows. Thus the reactor can be moved independently from the optical cavity.

An optical parametric oscillator (OPO) pumped by a Nd:YAG laser (Quanta-Ray PRO and MOPO-HF, Spectra Physics) with a repetition rate of 10 Hz and a bandwidth of $< 0.1\,\mathrm{cm}^{-1}$ is used as the light source. A combination of a Galilean telescope with a pinhole (200 μm in diameter) and an iris aperture in front of the input mirror to decrease the beam spot size to approximately 2 mm causes the preferential excitation of the TEM_{00} mode (Fig. 2). The light exiting the cavity is detected by a photomultiplier (PMT) (EMI 9558QB) operated at voltages between 700 and 800 V.

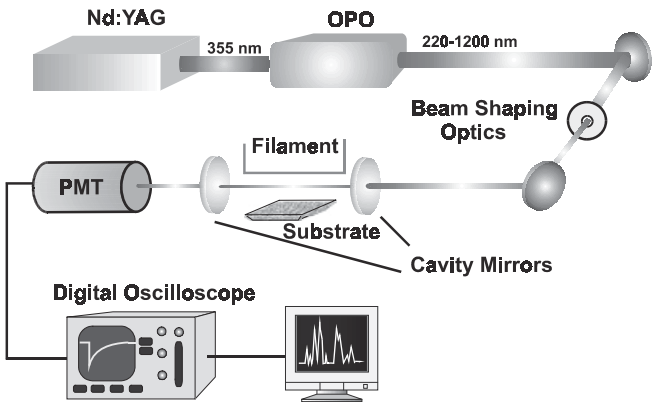

Fig. 2. Schematic of the experimental setup

Emission from the filament and the residual idler output of the OPO is blocked by a hot ($\lambda_{\mathrm{transmission}} < 750$ nm) and a blue filter in front of the PMT. The unamplified output of the PMT is recorded by a digital oscilloscope (HP 54510 A, analog bandwidth 1 GHz, vertical resolution 8 bit). The digitized data are transferred via the IEEE-488 interface to a personal computer. Using the LabVIEW virtual instrument software package (National Instruments Inc.) the ring-down lifetime is derived from the slope of a semi-logarithmic plot of the decay trace. Only the portion of the ring-down signal between 90 and 10% of the maximum intensity is used in the fit to avoid interference from mode beating in the beginning and noise at the end of the ring-down. The fitting procedure is a standard linear least-square fit (error for τ is usually less than 0.3%). The average of approximately 10 data points prior to the start of the decay signal is taken as the baseline value and subtracted from the decay signal before fitting. The ring-down lifetime is then derived from averaging usually 30 individually fitted decay traces. The ring-down lifetime τ_0 is determined from the baseline (where the absorption coefficient $\alpha = \sigma \cdot N$ is approximately zero) of the Gaussian fit that is used to evaluate the absorption intensities.

2 Results

2.1 Spatial distribution of CH

Figure 3 presents the spatial distribution of the CH radical. The concentration is on the order of 10^{11} molecules/cm^3 and decreases with increasing distance from the filament. The concentration is determined from the $Q_{\mathrm{IIe}}(9)$ transition in the CH $A^2\Delta - X^2\Pi$ (0,0) band system at 430 nm using a procedure outlined in [6, 39]. The absorption cross section is calculated from the Einstein coefficient B_{12} from Luque and Crosley [40] taking into account the temperature-dependent Boltzmann factor. The qualitative trend of the concentration profile of CH resembles profiles for the H atom [7, 12, 17], but differs remarkably from the profile of CH_3, which shows a maximum at 5 mm from the filament [41].

2.2 Gas temperature in the reactor

It is essential to establish the temperature in the gas phase to correct the absorption cross section for temperature in the concentration measurements of CH and to provide a temperature profile for computational simulations. The temperature in the gas phase of the reactor is derived from a Boltzmann plot. This plot includes lines from members of the Q-branch with $N = 5 - 15$ of the CH A-X (0,0) band. Figure 4a shows an example of such a graph, where the line-strength-corrected intensities are plotted versus the (rotational) ground-state energies of the initial absorption level (Boltzmann plot). The linearity of the plot indicates rotational equilibrium for the CH molecule. The gas-phase temperature as a function of distance from the filament is shown in Fig. 4b. The temperature in proximity to the filament is 1500 K and drops at the most distant point of our measurements to 1200 K. The large temperature drop between the filament and the surrounding gas phase has been explained by the breakdown of the (continuum) energy conduction theory [6] and is in

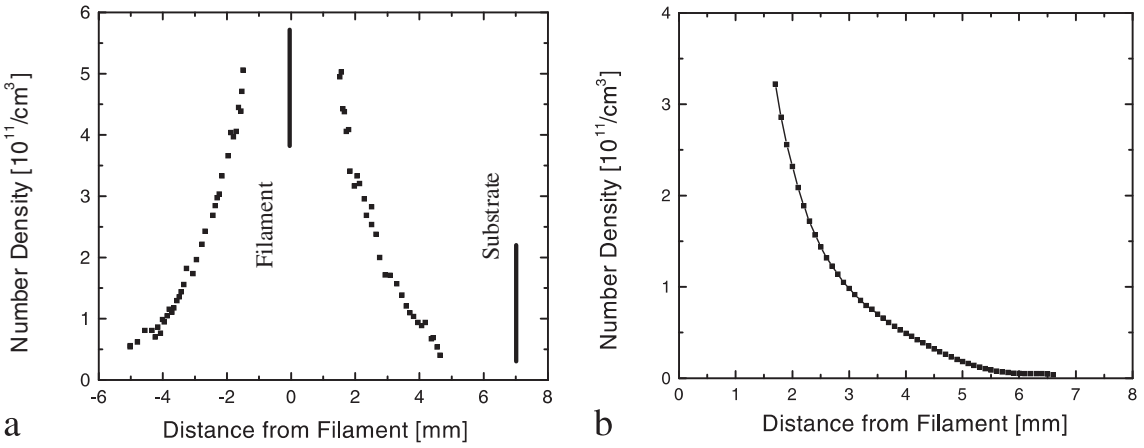

Fig. 3. a Concentration profile of the CH radical. The error in the CH concentration measurements is ∼ 25% and is mainly due to the uncertainty in the path length and the absorption cross-section [6]. The experiment is performed with the long axis of the filament parallel to the laser beam. The filament and the substrate are heated to a temperature of 2500 K and 1172 K, respectively. The CH_4/H_2 ratio is 0.01 and the pressure is 20 Torr. **b** Distribution of the CH radical after Abel inversion of the data to correct for the inhomogeneous distribution of the species along the line of sight. For this type of measurement the filament is perpendicular to the laser beam. Except for the absence of the substrate, the conditions are otherwise identical to **a**

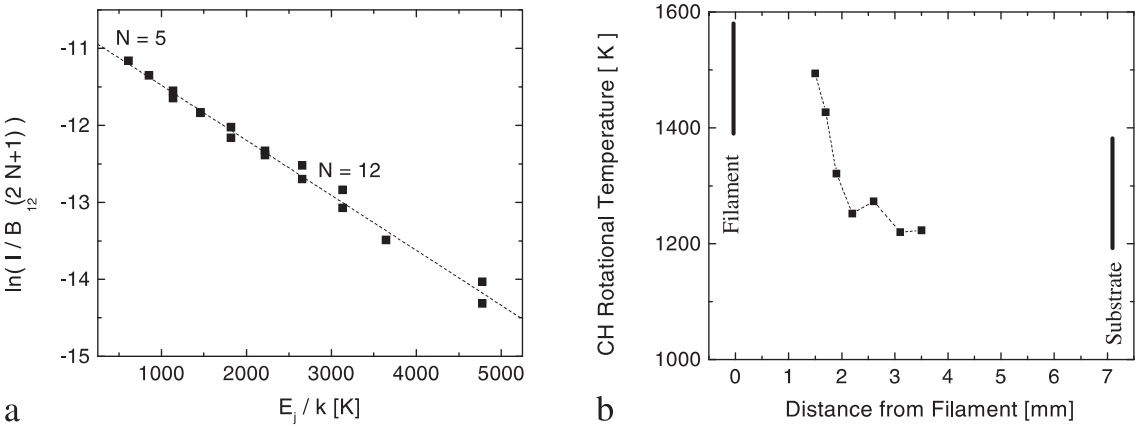

Fig. 4. a Boltzmann plot using transitions (with the rotational quantum number N) in the Q-branch of CH. **b** Rotational temperature of the CH radical as a function of distance from the filament at a temperature of 2500 K. Other process conditions are as given in Fig. 3

agreement with H-atom temperature measurements in other studies; see [17] and references therein. The similarity between the temperatures for the H and the CH radical indicates that the measured CH temperature is a good indicator for the temperature of the other gas-phase species. This behavior is expected for a CVD system running at 20 Torr owing to the large collision rate. The temperature profile of the CH radical is therefore representative for the temperature in the HFCVD reactor and can be used in simulations for modeling the temperature.

2.3 Substitution of H_2 *by* D_2 *in the feed gas*

To gain insight into the formation pathways of the CH radical an isotopic substitution experiment was performed. In the feed-gas mixture H_2 was substituted by D_2 (Cambridge Isotope Laboratories, Andover MA., isotopic purity 99.87%) while keeping all other parameters (e.g. filament temperature) constant with respect to the CH_4/H_2 measurements. Scanning the spectral range from 430 to 432 nm revealed none of the CH absorption lines (Fig. 5). From our estimated detection limit ($\alpha_{\mathrm{Min}} = 1 \times 10^{-8}\,\mathrm{cm}^{-1}$) we conclude that the CH concentration resulting from the CH_4/D_2 mixture is approximately smaller than 5×10^9 molecules/cm^3. Instead, new absorption features are found that are completely attributable to the A-X (0,0) band of CD [42]. The line positions are in excellent agreement with the available values derived from a dispersed emission spectrum by Geroe [43]. Herzberg also observed the CD A-X band in absorption but did not report line positions [44]. The number density of CD with the CH_4/D_2 mixture is comparable to the CH number density when using the CH_4/H_2 mixture, assuming the absorption cross-sections for CH and CD are similar.

2.4 Temporal study of CH *concentration*

Monitoring the CH absorbance in our reactor over extended periods of time shows a drastic difference in the temporal behavior for a tungsten filament compared to a rhenium filament. Figure 6 presents the measured absorbance from CH over a time period of ∼ 8 hours for both filament materials. While no significant change in the CH absorbance is observed for the tungsten filament, irregular (chaotic) oscillations are

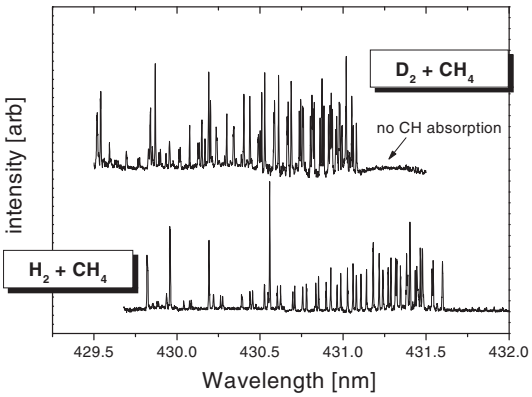

Fig. 5. CRDS scans of the spectral range from 432 to 429.5 nm (Q-branch region in the A-X (0,0) band of the CH and CD radicals) with a feed-gas mixture of CH_4/D_2 (*upper trace*) and of CH_4/H_2 (*lower trace*). The *upper trace* shows only transitions belonging exclusively to the CD radical. For comparison part of the absorption spectrum of CH when hydrogen is used instead of deuterium in the feed gas is shown in the *lower trace*. The filament temperature is 2500 K and the mixing ratio in the feed gas is 1% CH_4 in D_2 or H_2, respectively. The measurements were performed without a substrate in place

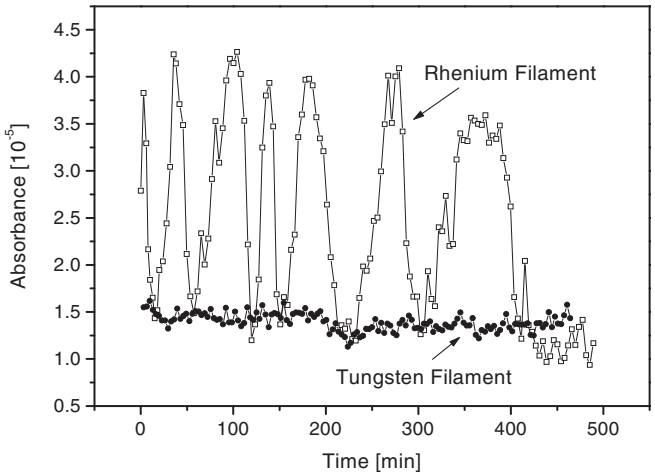

Fig. 6. Variation of CH absorbance over time using a rhenium filament (-□-) and a tungsten filament (-●-). Filament temperature is 2400 K and the measurement takes place at 2 mm distance from the filament. The absorbance is determined from the $Q_{II e}(9)$ transition, which is repeatedly scanned. The time for the measurement of each data point is approximately 3.5 min. This is the time required to scan the $Q_{II e}(9)$ peak. Similar oscillations were also observed with a mixing ratio of 0.5% CH_4 in H_2, at a flow rate of 50 sccm, at a filament temperature of 2500 K, and at locations 2.5, 3, and 4 mm from the filament. A substrate was not in place for these measurements

found for the rhenium filament. In the following it is assumed that the change in absorbance can be related to a change in CH number density (see below). With a quasi-periodicity on the order of minutes the CH concentration switches back and forth from a state of high to a state of low concentration. In Fig. 6 the low concentration level corresponds to the CH concentration found for the tungsten filament in Fig. 3, the high concentration level is approximately a factor of two larger. Both the period of the oscillations and the absolute values of the concentration levels were found to vary for multiple runs of the same experiment. This behavior is typical for a nonlinear system far from equilibrium, where slight changes in the initial conditions lead to strong changes in the dynamics of the system [45, 46].

Because the absorption cross-section is temperature dependent, the observed oscillations in absorbance could be related to a gas temperature change and not to a concentration change (c.f. (3)). To observe this large variation in absorbance a temperature change of the CH radical of more than 500 K is required (at constant CH concentration). This variation is unlikely as no change in filament temperature was observed. However, this conclusion might be affected by a change of emissivity of the rhenium filament if its surface composition changes (see below) [47]. But the analysis of the line width of the absorption transitions, which are primarily Doppler broadened, recorded at the high and the low concentration levels, also indicates no difference in temperature. Experimental instabilities as a reason for the oscillations, such as pressure fluctuations, can be excluded. We rule out this possibility because of the absence of oscillations in the measurements with the tungsten filament. Considering that we found the oscillations with the rhenium filament but not for the tungsten filament under a variety of different process conditions (flow rates, positions in the reactor), different rhenium filaments and different probed absorption lines, we believe that the temporal oscillations of the CH concentration is not likely to be an experimental artifact.

3 Discussion

3.1 Spatial distribution of CH

The spatially resolved concentration measurements of radicals are a test case for theoretical model calculations and provide insight into the chemical processes in a CVD reactor. From the computed diffusion length (travel distance between reactive collisions) on the order of millimeters for most hydrocarbon radicals [38], it follows that a specific CH radical away from a surface cannot have a direct heterogeneous origin. Therefore CH formation takes place predominantly in the gas phase. From the profile in Fig. 3 it can be concluded that the CH production rate is highest near or at the filament [6]. The trend of the CH concentration profile is similar to the profiles of the H atoms, which are formed by heterogeneous dissociation of H_2 at the filament [36]. This might indicate that, in addition to gas-phase production, CH formation also takes place to some extent heterogeneously at the filament. The low number density of CH in the gas phase is in agreement with theoretical predictions, which exclude CH as a precursor in the diamond growth [36].

3.2 Formation pathways of CH

The absence of CH when H_2 is replaced by D_2 in the feed gas (Fig. 5) indicates that substantial isotope exchange in the CVD reactor takes place. Considering our detection limit of 5×10^9 molecules/cm^3 of CH, however, we cannot discriminate between two possibilities: (i) the CH number density reflects an isotopic ratio of CH/CD according to the H/D ratio in the feed gas, or (ii) the CH number density is substantially lower than this equilibrium value.

In case (i) a uniform and nonbiased distribution of H and D should give rise to 2% CH in the total amount of

methylidyne (CH/D) for a feed gas mixture of 1% CH_4 in D_2. The corresponding CH number density for a fraction of 2% is $\sim 5 \times 10^9$ molecules/cm^3. This value is derived from the measurements with a CH_4/H_2 mixture at the same conditions and assumes a complete (nonpreferential) scrambling between all species. In case (ii) H atoms would be trapped in molecules with reaction pathways that do not contribute significantly to methylidyne formation. Such a removal of H atoms from the methylidyne reaction cycle would then lead to a nonequilibrium isotopic distribution. As a result, a smaller amount of CH would be observed in the reactor than is expected from the total H/D ratio.

The experimental observation made here is in agreement with an isotope-exchange experiment for the CH_3 radical performed by Zumbach et al. [15]. In a similar experiment, where CH_4/D_2 was used as the feed gas, the only isotopomer of CH_3 that could be detected was CD_3. A detection limit for the different isotopomers was not given.

3.3 Nonperiodic temporal oscillations of CH *concentration*

The data in Fig. 6 show that under present process conditions, the CH concentration in our HF-CVD reactor with a rhenium filament is a bistable system, that exhibits nonperiodic transitions between the two states. The triggering event for these transitions appears to be the recurring formation and destruction of some sort of carbon layer (e.g. carbide) at the filament surface. Formation of carbon layers or carbides on rhenium filaments have been found in many studies [47–49]. However, oscillations in filament activity appear not to have been reported previously. In analogy to studies of CO oxidation on metal surfaces the formation and destruction of such a carbon layer might be induced by a surface reconstruction of the filament [50].

In principle the oscillations could be also related to a pure gas-phase mechanism. In a system, where gas-phase reactions, mass and energy transport are described by a large set of coupled differential equations, nonperiodic phenomena could easily be expected [45, 46]. However, the absence of oscillations in the measurements with the tungsten filament, which are identical to the rhenium measurements (except for the filament material) rule out this possibility. The data show clearly that without some 'irregularity' at the filament, no conditions in the gas phase exist which alone induce oscillations in the CH concentration. The origin of CH oscillations with the underlying mechanism of a nonperiodic change of the filament surface is also in agreement with results by Sommer and Smith [48]. They reported on the simultaneous existence of carbon-free and carbon-covered regions on a Re surface and a temperature-dependent conversion between both states of the filament.

The oscillations of CH concentration can be related to two different mechanisms, both having their origin in the temporal existence of a carbon layer at the filament surface. In the first mechanism the carbon layer at the filament surface alters the efficiency by which H_2 is dissociated in H atoms (H_2 dissociation mechanism). A change of the H production rate and therefore of the H/H_2 ratio in the gas phase influences via the hydrogen shift reactions (4) directly the CH concentration. A similar mechanism is well known as the so-called poisoning effect of the filament that occurs at high CH_4 ratios in the feed gas. At high CH_4 input ratios a decrease or termination in H-atom production (diamond growth) is observed and explained by the reduced ability (number of active sites) of the filament to dissociate H_2, which is caused by the formation of a carbon layer at the filament [36, 51]. The second mechanism relates the oscillations of the CH concentration to the evaporation of carbon-containing species, e.g., C or CH, from the filament (carbon evaporation mechanism). It has been observed by Winters et al. that a high carbon concentration at the filament surface leads to an increase of evaporation of carbon species [23]. This situation could be also interpreted as etching of the carbon layer by hydrogen atoms (e.g., forming CH among other species) in analogy to surface reactions of hydrogen and carbon at the substrate surface.

If the former mechanism is active, the low absorbance level should correspond to a carbon-covered filament and the high absorbance state to a highly efficient (pure) filament surface and vice versa in the latter case. Besides the possibility of a conversion between a clean surface and a carbon-covered surface, also a conversion between two different types of carbon covered surfaces is possible. A distinction between these mechanisms without in situ surface analysis of the filament is very difficult. A differentiation between both mechanisms is especially complicated by results from Gall et al. [49] which showed similar catalytic efficiency of rhenium for the pure metal, for a surface carbide and for carbon clusters bound to the surface but not for a graphite layer. These results suggest that in the case of the hydrogen-dissociation mechanism the nature of the carbon layer on the filament surface is graphitic because this type of surface is the only one to show a reduced catalytic efficiency. Even if the prevailing mechanism is a change in hydrogen dissociation efficiency, a contribution to the CH oscillations from carbon evaporation is likely however. We reach this conclusion based on the simple fact that the recurring destruction of the carbon layer must occur by evaporation of carbon species. Carbon diffusion into the bulk of the filament as a removal process seems to be unlikely, because no saturation effect was observed.

The difference between rhenium and tungsten can be also seen in the scanning electron microscopy images of both filament types, which were taken after approximately 30 h of use in the reactor (Fig. 7). Both filament materials resemble each other by exhibiting cracks that are induced by thermal stress and carburization. However, they differ in their surface morphology. Whereas the surface of the tungsten filament appears mostly regular, the surface morphology of the rhenium filament has a more pronounced nonuniformity. Those

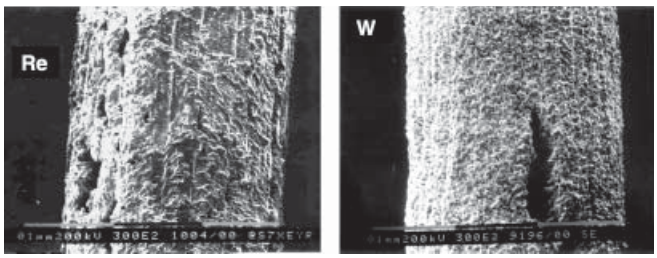

Fig. 7. Scanning electron microscopy (SEM) images of a rhenium (*left*) and tungsten (*right*) filament used in the reactor approximately 30 h under typical conditions. The images are taken at 20 kV at a magnification of ~ 3000

differences in surface appearance are another indication of a surface process causing the oscillations in CH absorbance.

This finding might have interesting implications for the diamond growth, which itself was not a subject of this investigation. A recent study [52] observed influences of a modulated CH_4 gas flow on the growth and nucleation of diamond, which allowed the synthesis of fractal carbon clusters.

4 Summary

Spatially resolved concentration and temperature profiles for the CH radical in a HF-CVD reactor are reported. The decrease of CH concentration with increasing distance from the filament is in agreement with a gas-phase production of this radical with the highest production rate very close to the filament. At locations close to the filament an additional contribution to CH production might arise from the filament evaporation of C_1 species (e.g. C atoms or CH) or from the dissociation of C_2 species at the filament. In an isotope-exchange experiment, where H_2 is replaced with D_2 in the feed gas, rapid isotope exchange is observed. The number density of CH in this experiment is equal or smaller to a CH/CD ratio corresponding to the total H/D ratio in the reactor. Resulting from this experiment the CRDS absorption spectrum of the CD radical is reported here. In a long-term study temporal oscillations in the CH concentration have been found, when a rhenium filament was used in place of a tungsten filament. The origin of these oscillations is attributed to two states of filament activity, which very likely correspond to the formation and destruction of a carbon layer at the rhenium filament. The large spatial gradients of concentration and temperature and the occurrence of nonlinear behavior are characteristic for a system far from equilibrium. Those nonequilibrium conditions are necessary to achieve growth of diamond under metastable conditions.

Acknowledgements. Uwe Lommatzsch gratefully acknowledges support from the Deutsche Forschungsgemeinschaft. The authors thank the Engineering Research Program of the Office of Basic Energy Sciences at the Department of Energy.

References

1. A. O'Keefe, D.A.G. Deacon: Rev. Sci. Instrum. **59**, 2544 (1988)
2. K.W. Busch, M.A. Busch (eds.): *Cavity-Ringdown Spectroscopy* (American Chemical Society Symposium Series 720, Washington 1999)
3. M.D. Levenson, B.A. Paldus, T.G. Spence, C.C. Harb, J.S. Harris, R.N. Zare: Chem. Phys. Lett. **290**, 335 (1998)
4. P. Zalicki, Y. Ma, R.N. Zare, E.H. Wahl, T.G. Owano, C.H. Kruger: Appl. Phys. Lett. **67**, 144 (1995)
5. R.L. Stolk, J.J. ter Meulen: Diam. Rel. Mater. **8**, 1251 (1999)
6. U. Lommatzsch, E.H. Wahl, T.G. Owano, C.H. Kruger, R.N. Zare: Chem. Phys. Lett. **320**, 339 (2000)
7. U. Meier, K. Kohse-Hoinghaus, L. Schafer, C. Klages: Appl. Opt. **29**, 4993 (1990)
8. E.A. Brinkman, G.A. Raiche, M.S. Brown, J.B. Jeffries: Appl. Phys. B **64**, 689 (1997)
9. J. Luque, W. Juchmann, J.B. Jeffries: Appl. Opt. **36**, 3261 (1997)
10. J. Cui, R. Fang: J. Appl. Phys. **81**, 2856 (1997)
11. S.O. Hay, W.C. Roman, M.B. Colket: J. Mater. Res. **5**, 2387 (1990)
12. K. Chen, M. Chuang, C.M. Penney, W.F. Banholzer: J. Appl. Phys. **71**, 1485 (1992)
13. F.G. Celii, J.E. Butler: J. Appl. Phys. **71**, 2877 (1992)
14. E.J. Corat, D.G. Goodwin: J. Appl. Phys. **74**, 2021 (1993)
15. V. Zumbach, J. Schaefer, J. Tobai, M. Ridder, T. Dreier, T. Schaich, J. Wolfrum, B. Ruf, F. Behrendt, O. Deutschman, J. Warnatz: J. Chem. Phys. **107**, 5918 (1997)
16. F.G. Celii, J.E. Butler: Appl. Phys. Lett. **54**, 1031 (1989)
17. S.A. Redman, C. Chung, K.N. Rosser, M.N.R. Ashfold: Phys. Chem. Chem. Phys. **1**, 1415 (1999)
18. L.L. Connell, J.W. Fleming, H.N. Chu, D.J. Vestyck, Jr., E. Jensen, J.E. Butler: J. Appl. Phys. **78**, 3622 (1995)
19. F.G. Celii, H.R. Thorsheim, J.E. Butler, L.S. Plano, J.M. Pinneo: J. Appl. Phys. **68**, 3814 (1990)
20. T.G. Owano, C.H. Kruger, D.S. Green, S. Williams, R.N. Zare: Diam. Rel. Mater. **2**, 661 (1993)
21. M.C. McMaster, W.L. Hsu, M.E. Coltrin, D.S. Dandy: J. Appl. Phys. **76**, 7567 (1994)
22. W.L. Hsu: Appl. Phys. Lett. **59**, 1427 (1991)
23. H.F. Winters, H. Seki, R.R. Rye, M.E. Coltrin: J. Appl. Phys. **76**, 1228 (1994)
24. S.J. Harris, A.M. Weiner, T.A. Perry: Appl. Phys. Lett. **53**, 1605 (1988)
25. H. Toyoda, M.A. Childs, K.L. Menningen, L.W. Anderson, J.E. Lawler: J. Appl. Phys. **75**, 3142 (1994)
26. K.L. Menningen, M.A. Childs, L.W. Anderson, J.E. Lawler: Rev. Sci. Instrum. **67**, 1546 (1996)
27. M.A. Childs, K.L. Menningen, L.W. Anderson, J.E. Lawler: J. Chem. Phys. **104**, 9111 (1996)
28. F.G. Celii, P.E. Pehrsson, H.T. Wang, J.E. Butler: Appl. Phys. Lett. **52**, 2043 (1988)
29. S.J. Harris, A.M. Weiner: J. Appl. Phys. **67**, 6520 (1990)
30. J.M. Larson, M.T. Swihart, S.L. Girshick: Diam. Rel. Mater. **8**, 1863 (1999)
31. P. Zalicki, R.N. Zare: J. Chem. Phys. **102**, 2708 (1995)
32. J.T. Hodges, J.P. Looney, R.D. van Zee: J. Chem. Phys. **105**, 10278 (1996)
33. K.K. Lehmann, D. Romanini: J. Chem. Phys. **105**, 10263 (1996)
34. M. Zhao, E.H. Wahl, T.G. Owano, C.C. Largent, R.N. Zare, C.H. Kruger: Chem. Phys. Lett. **318**, 555 (2000)
35. M.N.R. Ashfold, P.W. May, C.A. Rego, N.M. Everitt: Chem. Soc. Rev. **23**, 21 (1994)
36. D.G. Goodwin, J.E. Butler: In *Handbook of Industrial Diamonds and Diamond Films*, ed. by M.A. Prelas, G. Popovici, L.K. Bigelow (Marcel Dekker, New York 1998)
37. S.J. Harris, D.N. Belton, A.M. Weiner, S.J. Schmieg: J. Appl. Phys. **66**, 5353 (1989)
38. D.G. Goodwin, G.G. Gavillet: J. Appl. Phys. **68**, 6393 (1990)
39. E.H. Wahl, T.G. Owano, C.H. Kruger, U. Lommatzsch, D. Aderhold, R.N. Zare: Proc. Electrochem. Soc. **PV 99–32**, 80 (1999)
40. J. Luque, D.R. Crosley: J. Chem. Phys. **104**, 2146 (1996)
41. E.H. Wahl, T.G. Owano, C.H. Kruger, Y. Ma, P. Zalicki, R.N. Zare: Diam. Rel. Mater. **6**, 476 (1997)
42. G. Herzberg, J.W.C. Johns: Astrophys. J. **158**, 399 (1969)
43. I. Geroe: Zs. f. Phys. **117**, 709 (1941)
44. G. Herzberg: *Molecular Spectra and Molecular Structure I. Spectra of Diatomic Molecules* (Van Nostrand Reinhold, New York 1950)
45. G. Nicolis, I. Prigogine: *Self-organization in Nonequilibrium Systems* (Wiley, New York 1977)
46. H. Haken: *Synergetics: An Introduction: Nonequilibrium Phase Transitions and Self-organization in Physics, Chemistry, and Biology* (Springer, Berlin 1978)
47. P.G. Pallmer, R.L. Gordon, M.J. Dresser: J. Appl. Phys. **51**, 1798 (1980)
48. M. Sommer, F.W. Smith: J. Mater. Res. **5**, 2433 (1990)
49. N.R. Gall, S.N. Mikhailov, E.V. Rutkov, A.Y. Tontegode: Surf. Sci. **191**, 185 (1987)
50. R. Imbihl, G. Ertl: Chem. Rev. **95**, 697 (1995)
51. D.S. Dandy, M.E. Coltrin: J. Appl. Phys. **76**, 3102 (1994)
52. H. Zhai, C. Cao, H. Zhu, J. Li: Diam. Rel. Mater. **8**, 1891 (1999)